Soft Matter

PAPER

View Article Online
View Journal | View Issue



Cite this: *Soft Matter*, 2025, **21**, 7842

# Local deformation and dynamics of cross-linked hyaluronic acid gels at charged interfaces

Sujata Dhakal, Samyuktha Chandrasekar, Adediwura Deborah Adedeji and Svetlana Morozova *

Hydrogel adhesion is a complex process that involves chain dynamics, thermodynamics, chemistry, and topology. Using fluorescent confocal microscopy in combination with fluorescent differential dynamic microscopy (fDDM), we have determined surface deformation and dynamics of cross-linked hyaluronic acid (HA) gels, equilibrated against 1–1000 mM NaCl solutions, at positively and negatively ionized surfaces. Due to the negative ionization of HA, the gels are repelled from negatively ionized glass surfaces creating a fluid separation layer and repulsion remains unaffected by salt concentration. At these interfaces, the gel network motion is slowed, as determined with fDDM in 167 mM ionic strength. To create positively ionized surfaces, poly-L-lysine is deposited on the glass surface. At higher salt concentrations, surface ionization has little effect, while in lower salt concentrations, the softer gels are compressed 4–6 times by the surface forces. In lower salt concentrations, the surface interactions are less screened and the gels are softer, leading to greater deformation. These results reveal that gel deformation and interfacial dynamics are governed by a delicate interplay between gel modulus, surface ionization, and ionic strength, underscoring the need for new theoretical models to predict soft gel behavior at interfaces and enabling the rational design of gel-based adhesives, coatings, and biointerfaces.

Received 17th June 2025,
Accepted 16th September 2025

DOI: 10.1039/d5sm00616c

rsc.li/soft-matter-journal



## Introduction

Polymer gels consist of either a chemically or physically cross-linked polymer network swollen in a solvent.[1] The hybrid solid–liquid nature of these materials gives them unique properties and is what makes them fundamental to life and to many technologies.[1,2] For chemically cross-linked gels, the solvent swells the polymer network, which stretches the chains. This leads to an equilibrium where osmotic forces, polymer–solvent interactions, and chain stretching balance to determine the final polymer concentration inside the gel.[3–11] For charged gels, swelling is supplemented by Donnan equilibrium which adds an extra osmotic stress from the presence of dissociated ions at lower ionic strength.[12,13] At an interface, the gel state is complicated by the interaction with the surface, and the gel may adapt a new equilibrium.[14–19] This manifests in different phenomena, including lubrication, wet adhesion, gel adhesion, and de-wetting effects.[18,20–23] It has been shown that topology, surface interactions and mechanical effects all interplay at these boundaries, but direct measurement of surface gel dynamics has been challenging.[21,24]

The state of the gel at surfaces is complicated by the surface tension of the liquid and any adsorption or desorption of the chains. Molecular-level theoretical descriptions of the gel–solid interface are limited, but a scaling model based on repulsion and adsorption was developed by Gong *et al.*[25,26] Gong *et al.* have found that contact angle and surface interactions are critical parameters in gel lubrication/adhesion.[25] Hydrophobic surfaces and repulsive interactions typically correspond to a lower friction coefficient. They came up with a model that relates gel friction to either adsorption or repulsion of polymer chains at the surface.[26] For a strongly repulsive surface, there is expected to be a depleted layer on the order of the mesh size, $\xi$, and the interface surface energy of the liquid is balanced by the osmotic pressure of the gel.[26] When the polymers are attracted to the surface, they adsorb with an attraction energy, $F_{ads}$. The adsorption energy perturbs the interface at a characteristic length scale $R_a$ in the vertical direction, which depends on the gel osmotic pressure and the total adsorption strength. Their experimental results are similar to their model.[15,25,26] Others have also seen similar effects. Using micro indentation, Reale *et al.* found that more hydrated, unperturbed surfaces have a lower coefficient of friction.[18] The coefficient changes as the local polymer concentration changes with applied pressure, highlighting the unique and complicated behavior of gels at interfaces.[18]

The deformation of soft swollen gels can show complex surface interactions. One example of this phenomenon is gel phase separation at the liquid wetting ridge.[22] Ru *et al.* credit

*Department of Macromolecular Science and Engineering, Case Western Reserve University, Cleveland OH, USA. E-mail: sam381@case.edu*

the phase separation at the tip of the wetting ridge to the combined influence of the elastic forces, mixing effects, and interfacial attractions.[22] Jensen *et al.* studied the contact angle between a soft silicone substrate swollen in oil and rigid silica spheres and found that the material deforms fundamentally differently at the contact line than a non-gel solid due to the swelling of the gel.[27] When in adhesive contact, the contact geometry formed by the silica spheres at the gel interface is similar to liquid droplets, despite being solid.[27] Moreover, at high deformation, fluid is separated from the gel at the contact line. The amount of fluid that separates from the soft silicone substrate depends on the network's elasticity and the sphere's indentation.[27] This adhesion also affects the gel's local composition and thermodynamic behavior.[27] Jensen *et al.* suggest that hydrogels, being more compressible than silicone gels, may be even more prone to phase separation upon contact, despite being single-phase in bulk.[27] Cai *et al.* studied the deformation and phase behavior of soft polydimethylsiloxane (PDMS) networks swollen with silicone oil by water droplets.[28] These studies highlight that surface-induced deformation in swollen gels arises from a delicate and nonlinear interplay between network elasticity, osmotic pressure, and interfacial forces, suggesting that even nominally homogeneous gels can undergo local phase or structural rearrangements at interfaces which necessitates more nuanced models of soft adhesion and wetting.[27,28]

Hyaluronic acid (HA), a charged and highly hydrophilic polymer network found in the extracellular matrix (ECM), plays a key role in tissue lubrication.[29] HA creates a hydrating environment essential for the pliability and smooth movement of soft connective tissues.[30] The HA networks respond to various stimuli such as changes in temperature, pH, and ionic strength. Charged gels like HA consist of a cross-linked polymer network with fixed ionizable monomers that are balanced by mobile counter ions and can swell or shrink depending on the ionic environment.[7,31,32] The swelling behavior of the charged gels can be dictated by three factors, namely, solvent interactions, network elastic restoring forces and the osmotic pressure derived from the counter ions.[7,31,32] Decreasing the ionic strength and the cross-link density decreases the polymer volume fraction, leading to a softer and swollen gels.[7] Inversely, highly cross-linked gels have a high volume fraction and shear modulus, leading to a stiffer gel in comparison. However, for a constant cross-link density, the modulus can be nonmonotonic with ionic strength. In low ionic strength solutions, the osmotic pressure generated by the ionized backbone monomers remains significant and leads to increased swelling. In some cases, this osmotic pressure is so high that it increases the overall modulus of the gel.[33,34] This results in elevated Donnan osmotic pressure from counterions, leading to a more rigid network under low ionic strength conditions. In such environments, HA gels are expected to strongly interact with charged interfaces. In contrast, at high ionic strength, the ion pressure is low, resulting in a higher polymer concentration within the gel and again higher pressure.[32]

Hydrogel interfacial equilibrium and dynamics are key to understanding the response of soft systems to changes in the environment and can be used to engineer materials that interface with biological tissues and understand biological communication in elastic matrices. Since many hydrogel applications depend on surface interactions and response to external stimuli, a fundamental understanding of these interfaces is key to designing gels for advanced technologies.[35] The effect on deformation as a response to factors like ionic strength, cross-link density and surface ionization has yet to be studied. Here, we develop a system to study the interfacial dynamics of hydrogels and how it responds locally to a charged interface.

We have used fluorescence confocal microscopy to directly visualize HA gels in contact with repulsive surfaces as well as any gel deformation at attractive interfaces (Fig. 1). Fluorescent Differential Dynamic Microscopy (fDDM) is used to assess whether interfacial interactions affect polymer dynamics. To study negatively charged surfaces, we examine the HA gel equilibrium concentration with confocal microscopy and dynamics with fDDM near etched glass slides. To study positively charged surfaces, the glass slides were modified by introducing a thin layer of positively ionizable poly-L-lysine (PLL). The new local equilibrium is established based on the interaction with the surface, and the deformation is related to the modulus and ionic environment. These results provide the first direct, simultaneous visualization of how surface charge and gel mechanics reshape local equilibrium at soft interfaces. This work establishes experimental benchmarks for theoretical models of gel–solid contact and offers design insights for engineered biointerfaces, adhesives, and lubricious coatings.

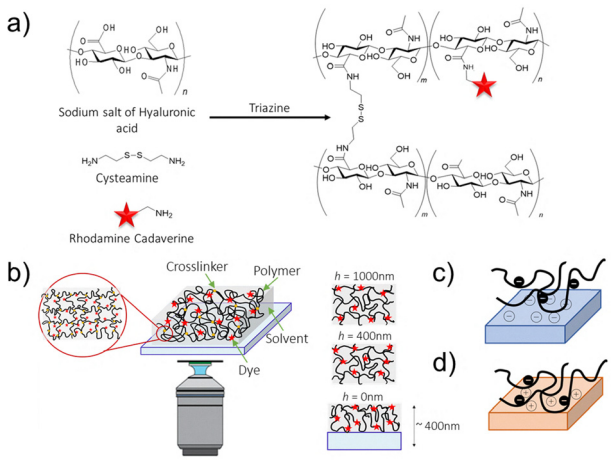


Fig. 1 (a) Schematic diagram showing the chemical cross-linking and fluorescent dye conjugation of HA gels. (b) fDDM setup depicting its ability to image at the interface and move in the *z* axis to capture extended effect of surface interaction up to the bulk. (c) Negatively charged surface interacting with negatively charged HA gel. (d) Positively ionized surface modified with PLL interacting with negatively charged HA gel.

## Materials and methods

### Materials

Sodium hyaluronate (NaHA) was purchased from Lifecore Biomedical ($M_w$ ~ 1 500 000 Da). Cystamine dihydrochloride,

poly-L-lysine ($M_w$ > 300 000 Da) and all salts were purchased from Sigma-Aldrich. Tetramethylrhodamine cadaverine (RhB) was purchased from Invitrogen. 4-(4,6-Dimethoxy-1,3,5-triazine-2-yl)-4-methylmorpholinium chloride (DMTMM) was purchased from TCI. All chemicals were used without further purification. Ultrapure de-ionized water from Milli-Q® IQ water systems was used throughout.

### Gel preparation

To synthesize the gels, 10 mg NaHA was dissolved in 1 mL DI water and heated at 60 °C to aid dissolution. 0.5 molar% and 1 molar% cysteamine was added as the cross-linking agent. To increase the contrast of the system, 150 μL of 5 mg $mL^{-1}$ RhB was added to each vial(Fig. 1). To gel the solutions, 30 mg of triazine was then added. Triazine (DMTMM) functions as a coupling agent by initially activating a carboxylic acid group on the HA chain, creating a reactive intermediate.[36–39] It then promotes the reaction of this intermediate with an amine (from cysteamine), leading to the formation of the new bond. The solutions were left inside a dark cabinet for ~24 h to cure. After gelation, all gels were swollen in 1 mM, 10 mM, 50 mM, and 1 M NaCl, as well as in phosphate buffered saline (PBS) with an ionic strength of 167 mM and at pH 7.4. The swelling solutions were changed periodically over the course of two days to get rid of any unreacted molecules and excess dye.

### Confocal imaging

Number 1 coverslips were cleaned sequentially with soap and water, followed by acetone, rinsed with deionized water and then dried using house air. The coverslips were then etched with ozone in a Jelight UV-Ozone model 24 for 30 minutes. The glass coverslip has a typical bare charge density of ~−10 mC $m^{-2}$.[40] This is due to the hydroxyl (–OH) layer on the glass surface making it negatively ionized.[41] To make the surface positively ionized, the Ozone-treated glass coverslips were then submerged in 1 mg $mL^{-1}$ poly-L-lysine (>300 000 Da) for ~5 min and dried using house air. A chunk of gel, approximately 10 mm by 10 mm was placed on either the negatively or the positively ionized coverslip and any excess water was dried off using Kim wipe.

For confocal experiments, the glass slide was set up on a Leica DMI 4000B microscope sample stage. A 100× objective was used to focus on the gel surface at interface. Images were taken from the interfaces to 5 μm into the bulk at an interval of every 0.21 μm. At each interval, 10 images were averaged. The intensity as a function of height was then plotted and normalized. For this process, 1 wt% solution of HA was prepared with 150 μL of 5 mg $mL^{-1}$ RhB, followed by capturing confocal images of the solution as a function of height. The intensity values at each height obtained from these images served as a reference. The intensity of each gel was normalized by the reference at each height. This step corrected the variations in intensity caused by differences in scattering and optical effects as a function of distance into the sample. Next, to account for any changes in intensity due to difference in dye concentration due to swelling or variations in conjugation percent, the intensity data were further normalized by the bulk gel intensity at a reference height of 3 μm. This reference value helped standardize the measurements, ensuring that any variation in intensity due to the gel's optical properties was properly accounted for. Intensities from at least 4 different spots within the image were averaged to minimize the optical variation from surface textures.

### Differential dynamic microscopy

For the fluorescence differential dynamic microscopy (fDDM) experiments, the gels were placed on the coverslip and set up on the Leica DMI 4000B microscope similar to the confocal setup. A 100× objective was used to focus on the surface and .avi videos were taken at the surface, 200 nm, 400 nm, 1000 nm, and 2000 nm into the bulk. The gel network dynamics can be determined by tracking the fluctuation in intensity in each of the images and auto correlating them in Fourier space using an in-house Matlab code. The Intermediate Scattering Function, $g_1$ is derived from the cooperative thermally excited fluctuations of the chemically cross-linked HA gels. Tanaka *et al.* explained that fluctuation arises from the thermally excited density fluctuations in the polymer network.[42,43] The fluctuations are linked to the displacement vector, $u$, and at equilibrium, the cooperative motion of the gel strands can be described as:

$$f\frac{\partial u}{\partial t} = \left(K_0 + \frac{1}{3}\mu\right)\nabla(\nabla \cdot u) + \left(\mu\nabla^2 u\right) \quad (1)$$

where, $f$ is the friction coefficient of the network against the solvent, $K_0$ is the osmotic modulus, and $\mu$ is the shear modulus. The displacement vector, $u$, has an ensemble average of zero, *i.e.* $\langle u(\mathbf{r},t)\rangle = 0$. However, the intermediate scattering function is proportional to the density fluctuations and can be described as:[34,43]

$$g_1 = \exp - D_e q^2 \Delta t \sim \langle u(q, 0)u(q, \Delta t)\rangle \quad (2)$$

where $q$ is the wave-vector that corresponds to the inverse spatial position in the image, $q = 2\pi\sqrt{u_x^2 + u_y^2}$ with $u_x$ and $u_y$ corresponding to the coordinates of the image in the Fourier space, $\Delta t$ is the time lag, and $D_e$ is the collective diffusion coefficient of the polymer solution or gel. In gels, $D_e$ is the "elastic" diffusion coefficient. For solid, chemically cross-linked gels, $D_e$ is related to $K_0$, $\mu$, and $f$, $D_e = \dfrac{K_0 + \left(\frac{4}{3}\right)\mu}{f}$, and is related to the pressure wave motion in the solid material.[36,43]

fDDM captures intensities as a function of time and relies on autocorrelating intensities in Fourier space to determine the dynamics of the system. Hydrogels are heterogeneous in nature and there are areas of varying cross-link densities within the system. Due to the heterogeneity, we expect that each surface location has a slightly different elastic diffusion coefficient, but we note that the advantage of fDDM is obtaining local dynamics at a specific height away from the surface. The ensemble average of the network fluctuation from image to image results in a function that holds the information about the systems relaxation

 

$$C = A(q)(1 - g_1(q, \Delta t)) + B(q) \quad (3)$$

where $A(q)$ is dependent on the optical transfer function and scattering properties of the objects, $B(q)$ captures the background of the system, and the intermediate scattering function, $g_1(q, \Delta t)$, carries information about the system relaxation. The ISF function is then fit with single or multiple relaxation rates, $\Gamma$, which are plotted against $q^2$ and fitted linearly to obtain the diffusion coefficient of the network.[44–49]

## Results and discussion

Confocal images were taken as a function of height, $h$, and surface modification (Fig. 2) to determine the local deformation due to surface interactions. UV-Ozone etched glass was used for negatively ionized surfaces and positively charged surfaces were prepared by depositing PLL onto the cover glass (Fig. 2a). The representative micrographs are shown in Fig. 2b and c for negative surfaces and positive surfaces. In Fig. 2b and c, we show that the intensity of the gel is brightest within 400 nm and then decreases further into the gel near attractive surfaces in 167 mM ionic strength. In contrast, the intensity near the negatively charged surface is much lower and increases slightly away from the surface. From the 3D image obtained from all the confocal micrographs, the results show that for an unmodified surface, adsorption is lower than that for the PLL covered surface (Fig. 2c). In Fig. 2d, we summarize this effect by plotting the average intensity of 4 different locations within each gel as a function of height away from the surface for 1% and 0.5% cross-linked gels at negative and positive glass in phosphate buffered saline (~167 mM), after accounting for optical scattering by normalizing the intensity by a constant concentration of dye (125 μL of 0.5 mg mL$^{-1}$) at the same height. The peak deformation from the attractive interface is 1.5 times for 0.5% cross-linked gels, and 1.2 times for 1% gels at a constant ionic strength. Since 1% gels are more concentrated in equilibrium, they are harder to deform. Similarly, near repulsive surfaces, the decrease in intensity is much more for the lower cross-linked gels on average. These results demonstrate that the extent of surface-induced deformation is modulated by both the charge of the surface and the gel's cross-linking density and that the deformation is greater for softer gels.

### Effects of ionic strength

To determine the effects of ionic strength, both the 0.5% and 1% gels were further swollen in 1 mM 10 mM, 50 mM, 1X PBS (~167 mM NaCl), and 1 M NaCl and the resulting deformation was measured as a function of height using confocal imaging.

In Fig. 3, we show that the deformation is directly related to both the surface ionization and the salt concentration. Fig. 3a and b show the repulsion effect on the surface for all salt concentration for both gels. The low intensity at the surface is from the presence of a water layer between the glass and the gel. This phenomenon has also been observed for silicone oil systems.[23,27,28] Due to the repulsion, the polymer network is pushed away from the surface, creating a water layer as a buffer at the interface. This is supported by Fig. 2c where an uneven layer of minimal intensity is evident. The formation of the water layer is mostly independent of the modulus and the salt concentration (Fig. 3a and c). However, as shown in Fig. 3a and b, in 1 M NaCl, the gels are much closer to the surface despite the presence of the water layer (Fig. S2a and S4a). It can be noted that the repulsive effect diminishes at high salt concentration.

The interaction near attractive surfaces is drastically different from the fluid separation at repulsive surfaces. The peak in intensity near an attractive surface is evidence of deformation. We assume that the dye's fluorescence intensity in confocal images correlates directly to the concentration of the HA network. Therefore, an increase in normalized intensity relative to the background indicates a higher local concentration of the network. This allows us to infer that the regions with increased intensity are areas where gel is "compressed". As seen from Fig. 3c and d, the deformation is a function of surface ionization, salt concentration, and cross-link density. For 0.5% cross-linked gels, the deformation in 1 mM is ~6 and decreases to ~1 in 167 mM. This trend is persistent for all salt concentrations. At the highest salt concentration, there is no intensity peak near the surface. For 1.0% cross-linked gels,

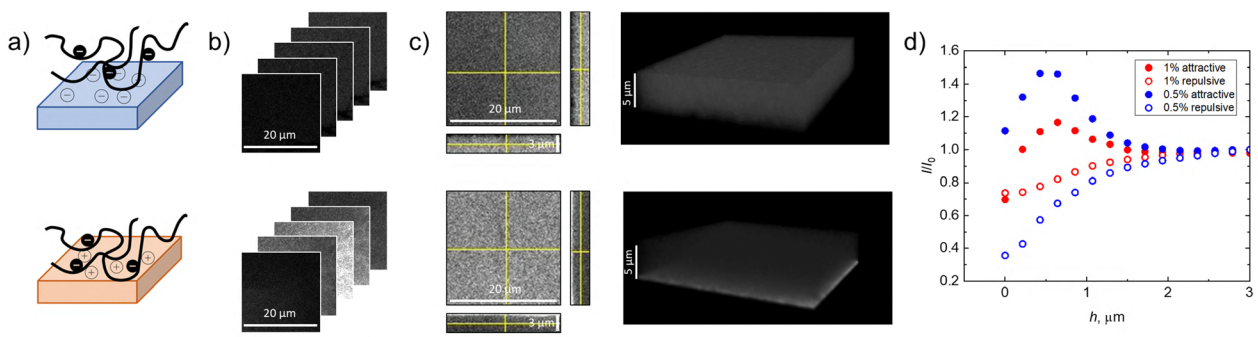


Fig. 2 (a) Negatively modified surface (top), and positively modified surface (bottom). (b) 2D stack of confocal images at different heights, h, for repulsive surfaces (top) and attractive surfaces (bottom), $\Delta h$ = 0.21 μm. (c) 2D orthogonal view and 3D representation of the gel for repulsive surfaces (top) and attractive surfaces (bottom). (d) Normalized intensity *vs.* height obtained from confocal imaging for attractive, PLL surfaces and repulsive, unmodified surfaces.

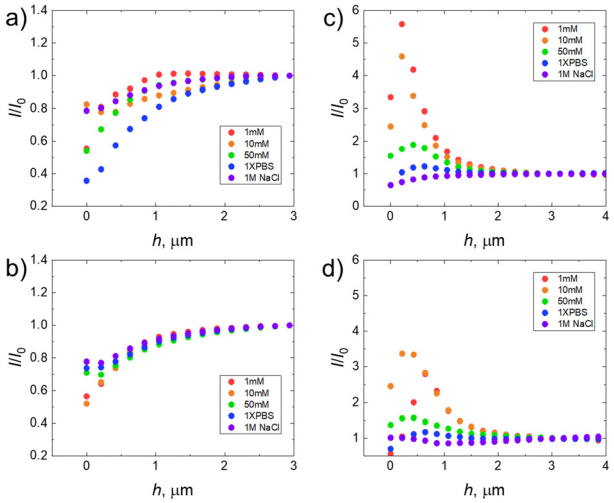


Fig. 3 Normalized intensity of HA gels as a function of salt concentration at different cross-link densities and surface ionization. (a) 0.5% cross-linked gel at repulsive surfaces. (b) 1.0% cross-linked gel at repulsive surfaces. (c) 0.5% cross-linked gel at attractive surfaces, and (d) 1.0% cross-linked gel at attractive surfaces.

the deformation is lower compared to 0.5% cross-linked gels. At 1 mM, the deformation is ~2.5 which is half that of the 0.5% cross-linked gel at the same ionic strength. In addition, the effect is non-monotonic with ionic strength. The cross-link density trend and the salt trend can be attributed to the swelling equilibrium modulus of the gels. Hydrogels with low cross-link density have a lower elastic modulus and can swell extensively and retain large amount of water. In contrast, hydrogels with high crosslink density possess a denser network structure, making them stiffer and less capable of swelling. This inverse relationship between crosslink density and swelling behavior highlights the critical role of network architecture in determining hydrogel deformability.

Frequency sweep data were measured to determine the modulus, $G'$, of the gels as a function of ionic strength. After swelling the gels in different salt concentrations ranging from 1 mM to 1 M for at least 24 hours, we find that the modulus increased as a function of salt concentration for 0.5% cross-linked gels and is non-monotonic as a function of ionic strength for 1% cross-linked gels (Fig. 4). For 0.5% cross-linked gels, lower ionic strength leads to greater swelling and correspondingly, a lower modulus. The modulus then increases from $G' \sim 10$ Pa in 1 mM to $G' \sim 50$ Pa in 1 M, as the gel concentration increases. For 1.0% cross-linked gels, the trend is non-monotonic, as has been reported previously.[34,50] For 1.0% cross-linked gels, $G'$ varies with ionic strength: $G' \sim 50$ Pa in 1 mM NaCl, $G' \sim 25$ Pa in 10 mM, $G' \sim 40$ Pa in 50 mM, $G' \sim 105$ Pa in 167 mM and $G' \sim 110$ Pa in 1 M. There is a clear trend in the modulus and the cross-link densities of the gels. The lower cross-link density gels are softer for all ionic strengths and deform more as evident from the rheological data and confocal microscopy. The effect as a function of ionic strength is non-monotonic for higher cross-linked gels due to the internal equilibrium of the gels.

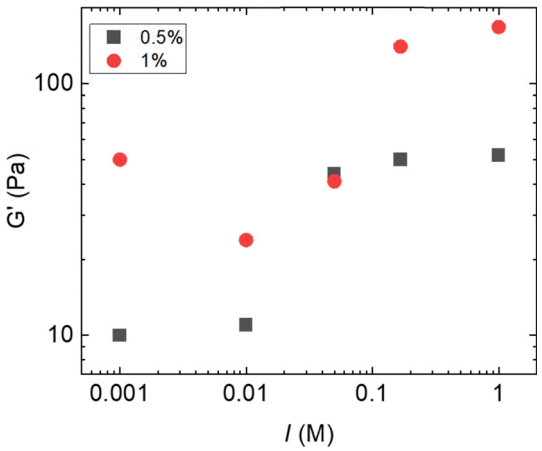


Fig. 4 Elastic modulus of 0.5% and 1.0% cross-linked HA gels as a function of salt concentration.

For a constant surface charge density, the deformation by the surface is an inverse function of the gel modulus. The pressure exerted by a charged wall separated by a monomer distance $\sim d \sim 1$ nm is given by:[51]

$$P_e = \sigma_g \sigma_s \, e^{(-\kappa d)}/(2\varepsilon) \quad (4)$$

where $\sigma_s$ is the glass surface charge density, $\sigma_g$ is the gel surface charge density, $\kappa$ ($nm^{-1}$) is the inverse Debye screening length, equal to $\sim \sqrt{I(M)}/0.304$ in water, $\varepsilon$ is the permittivity of the medium, and $I$ is the ionic strength.

The electrostatic pressure is counteracted by the modulus at the interface:

$$P_e = (\Delta\varphi/\varphi)K \quad (5)$$

where $\Delta\varphi/\varphi$ is the relative compression at the interface and $K$ is the compression modulus, proportional to the shear modulus by a factor of $2/3(1 + \nu)/(1 - 2\nu)$, where $\nu$ is Poisson's ratio.[52] Therefore, the deformation at the surface, should be directly inversely proportional to the shear modulus.

In addition, these two are relatively equal when $G' \sim 50$–$140$ Pa which corresponds to a compression modulus of $K \sim 10^4$ Pa for a nearly incompressible solid with $\nu = 0.499$, as measured previously.[34] This is consistent with an effective surface charge density of $\sim -9$–$15$ mC $m^{-2}$, which is on the order of typical values of the surface charge density of glass.[40] The deformation from the surface is directly related to the change in modulus for both gels. The slight difference in the amount of deformation by the surface at a similar modulus is consistent with the difference in gel concentration, and therefore $\sigma_g$.[53] As the gel swells, the polymer network expands and the volume fraction of the polymer decreases. Since the total number of fixed charges on the polymer backbone remains constant, the effective surface charge density ($\sigma_g$) at the gel interface boundary increases proportionally with the local polymer volume fraction. If we assume a constant surface charge density of 10 mC $m^{-2}$, the estimated $\sigma_g$ is 10 mC $m^{-2}$ for 0.5% and 26 mC $m^{-2}$ for the 1% gel, which matches the expected change due to swelling.[34]

A negatively charged polyelectrolyte gel with low cross-link density, swollen in low salt concentration, has a low modulus due to high swelling driven by counterion osmotic pressure and electrostatic repulsion between charged groups in the network.[53] The low ionic strength results in a long Debye length, allowing the electrostatic attraction to the positively charged surface to act over long distances. Local chains are drawn toward the surface, leading to adsorption. Deformation in this case is driven by a balance of electrostatic attraction and network elasticity.[53]

In contrast, a similar gel with high cross-link density is stiffer due to its denser network. Although the Debye length remains long in low salt concentrations, the stiffer network resists deformation more effectively. While surface attraction still induces deformation, it is slightly reduced compared to the softer gel due to the gel's greater mechanical resistance to spreading and chain extension.

Moreover, near repulsive surfaces, $P_e = \sigma_g\sigma_s\, e^{(-\kappa\xi)}/(2\varepsilon)$, where the separation is approximately the mesh size of the gel, $\xi$. In high salt concentrations, the repulsion is screened and the gel is able to get in close contact with the surface (see Fig. S1b and S2b).

DDM was used to determine the effects of surface ionization on the local dynamics as a function of height. Fig. 5a is a representative graph of the correlation functions. The correlation functions at each $q$ are fit to determine the relaxation rate, $\Gamma$, which is plotted against $q^2$ as shown in Fig. 5b and c and linearly fitted to determine the diffusion coefficient, $D_e$. The measured diffusion coefficient provides insight into the mobility of the tracer molecule (RhB dye) within the matrix and, by extension, the random motion of the polymer chain. Since $D_e = \dfrac{K_0 + \left(\frac{4}{3}\right)\mu}{f}$, a lower diffusion coefficient typically indicates a lower modulus or higher friction coefficient for the gel strands. In Fig. 5d, our findings reveal that the elastic diffusion coefficient ($D_e$) of the gels increases as a function of height, indicating that the network is free to fluctuate but the dynamics are slower at the surface compared to the bulk. This effect is much more pronounced for the 1% gels compared to the 0.5% gels likely because the hydration layer is hypothesized to be on the order of the mesh size, which is lower for the 1% gels, and the strands are close to the surface, which increases local friction. However, for PLL-treated surfaces, the local dynamics were unresolvable until 1 μm into the gel, at which point $D_e$ is larger than in the bulk, as measured with DLS. This can be attributed to a solid contact formed at the surface, which is difficult to resolve with fDDM. In this scenario, we expect that the molecular motion is matched between the glass and the gel, depending on the strength of the contact. While we do not expect slow dynamics of any movement over the long times, there likely is still molecular motion that depends on the strength of contact and the modulus of the glass, which cannot be captured with fDDM. For 1.0% cross-linked hydrogels, the apparent diffusion coefficient at the surface is $D_e = 4.0 \times 10^{-12}$ m$^2$ s$^{-1}$ which increases to $D_e = 16.2 \times 10^{-12}$ m$^2$ s$^{-1}$ at 400 nm away from the surface and $D_e = 17.6 \times 10^{-12}$ m$^2$ s$^{-1}$ at 1000 nm from the surface. Similarly, for 0.5% cross-linked hydrogels, the apparent diffusion coefficient at the surface is $D_e = 9.7 \times 10^{-12}$ m$^2$ s$^{-1}$ which increases to $D_e = 13.3 \times 10^{-12}$ m$^2$ s$^{-1}$ at 400 nm away from the surface, $D_e = 12.8 \times 10^{-12}$ m$^2$ s$^{-1}$ at 1000 nm from the surface, and $D_e = 12.2 \times 10^{-12}$ m$^2$ s$^{-1}$ at 2000 nm from the surface. The bulk values are expected from previous dynamic light scattering results.[34] In Fig. 5b, the error bars are an average of three runs. In Fig. 5d, the error bars are from the linear fits and increase as a function of height because the signal diminishes into the gel.

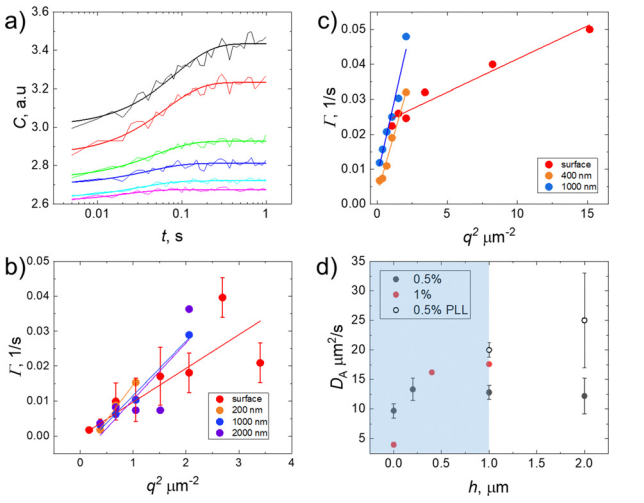


Fig. 5 (a) Autocorrelated intensity plotted against time and fitted with single exponential function to obtain the relaxation rate, $\Gamma$. (b) The relaxation rate plotted against $q^2$ and fitted linearly to obtain the diffusion coefficient for 0.5% cross-linked HA gel (swollen in 1X PBS) at a repulsive glass surface. (c) The relaxation rate plotted against $q^2$ and fitted linearly to obtain the diffusion coefficient for 1.0% cross-linked HA gel (swollen in 1X PBS) at a repulsive glass surface. (d) Diffusion coefficient as a function of height into the gel.

To further understand the role of electrostatic interactions at gel interfaces, we analyzed gel behavior close to attractive and repulsive surfaces in different ionic strength conditions, as shown in Fig. 6. Both parameters critically influence the adhesive and repulsive interactions of HA hydrogels. When a negatively charged HA gel is placed against a similarly negatively charged surface, repulsion dominates and the gel intensity near the interface remains consistently low across all salt concentrations, indicative of a persistent hydration layer that prevents close contact (Fig. 6a). In contrast, interactions with positively charged surfaces yield markedly different behavior, strongly modulated by ionic strength (Fig. 6b).

At low ionic strength, HA gels are more swollen and are softer, allowing significant deformation at the attractive interface. As ionic strength increases, the gel becomes more concentrated and stiffer, reducing the extent of surface-induced deformation. In intermediate salt concentrations, the gel remains sufficiently compliant to deform at the interface, although to a lesser degree than at low ionic strength, indicating that attractive interactions still influence the network.

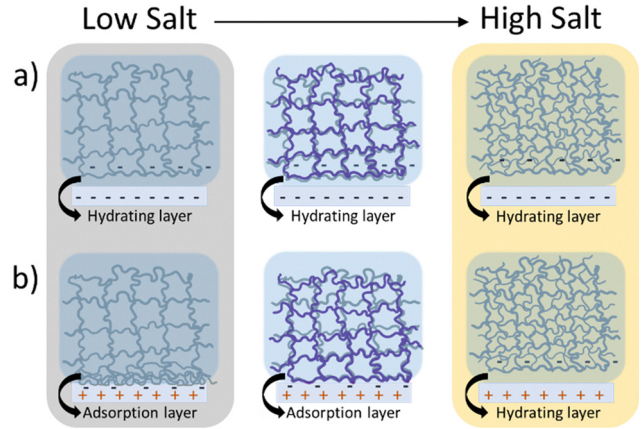


Fig. 6 Schematic representation of the effect of surface charge for (a) Repulsive, negatively ionized surface and (b) PLL-modified, positively ionized surface as a function of ionic strength. In intermediate salt concentration, where dynamics are resolvable, motion is slower near repulsive surfaces and no dynamics are resolvable at attractive surfaces.

Confocal results in Fig. 3c and d, corresponding to 0.5% and 1.0% cross-linked gels, respectively, confirm that deformation decreases with both increasing crosslink density and salt concentration. These trends are in agreement with prior theoretical and experimental studies which have shown that interfacial interactions can significantly alter soft gel structure. For instance, Gong *et al.* predicted surface behavior based on gel modulus, while Cai *et al.*, demonstrated that fluid migration and wetting ridge formation are influenced by swelling and cross-linking degree.[26,28] Others have shown that the modulus changes at an interface either by de-wetting effects or adhesion.[22,23,26,54] Our results support these conditions in the context of charged biopolymer networks, where electrostatic interactions and swelling behavior jointly determine interfacial deformation.

In intermediate salt concentrations (Fig. 6, middle panel), we analyzed the dynamics of negatively charged HA gels on both attractive (PLL-coated) and repulsive (unmodified) glass surfaces. At repulsive interfaces, two consistent observations emerge: (1) the apparent diffusion coefficient, $D_e$, decreases near the surface and (2) the confocal signal intensity is reduced, suggesting a lower local polymer concentration. This supports the presence of a depletion zone or ''hydrated layer'' as described by Gong *et al.*, where interfacial water separates from the network, leading to slowed dynamics (Fig. 5a).[25,26] In contrast, at attractive PLL-modified surfaces, the intensity is higher near the surface, which decays into the bulk, consistent with gel adsorption. No measurable dynamics were detected in these regions, implying that the HA chains may be immobilized at the surface or exhibit dynamics that are too rapid to resolve with fDDM. Although we are able to obtain local gel dynamics of soft hydrated HA gels near interfaces, there are limitations to fDDM in these systems. First, for most gels, the density fluctuations increase with increasing modulus, which may be beyond the time resolution of the 100 fps camera imaged at 100×. As the limit of temporal and spatial resolution is reached, it becomes much harder to determine if the dynamics are isotropic or heterogeneous. Another geometric limitation of the set up is observing the dynamics in the *z*-direction, which may be determined if the gel interface is rotated vertically, such that the interface is directly in plane in the imaging surface. Despite the limitations, there are many fundamental opportunities that are enabled with this imaging technique to study soft complex solid materials.

## Conclusions

We have used confocal microscopy to visualize the effects of surface ionization and salt concentration on HA hydrogel networks. The interaction at the interface is dependent on factors like cross-link density, surface ionization, salt concentration, and modulus. Interfacial deformation is strongly dependent on gel stiffness and ionic strength. The softer gels at low ionic strength exhibit pronounced deformation at attractive surfaces, which diminishes as gel modulus increases with salt concentration. In contrast, repulsive surfaces maintain a stable hydration layer at the interface, with no significant deformation across conditions. We also used fDDM to determine the dynamics of HA gels as a function of height away from charged surfaces. It revealed that the dynamics are slower near repulsive surfaces, increasing with distance into the bulk. For attractive surfaces, diffusion was below the resolution limit of our setup, likely due to restricted mobility from surface adsorption and formation of solid contact. These findings demonstrate that both deformation and dynamics at hydrogel interfaces are governed by a complex interplay of electrostatic interactions, mechanical properties, and ionic environment.

A thorough understanding of the interfacial dynamics of hydrogels is critical for advancing their use in a wide range of applications, particularly those involving complex environments. Hydrogels, being highly responsive to external stimuli such as change in ionic strength, pH, or mechanical stress, exhibit unique behaviors that are closely tied to internal structure and surface properties. By systematically varying surface and gel parameters, our work provides new insights into how interfacial properties of HA hydrogels can be modulated. This level of control is critical for the design of hydrogels in applications where surface adhesion, responsiveness, and interfacial mechanics are key, such as in bio interfaces, soft robotics, and drug delivery systems.

## Author contributions

S. M. conceptualized the project and S. D. designed and conducted the confocal and DDM experiments. S. C. helped with gathering confocal results and A. D. A. helped with rheological results. S. D. analysed and validated the results. S. D. wrote the manuscript and S. M. reviewed and edited the manuscript. All authors have read and agreed to the published version of the manuscript.

## Conflicts of interest

The authors declare no competing interest.

## Data availability

All raw confocal and DDM data, description and examples of image analysis can be downloaded on Open Science Framework: **https://osf.io/s8mwp/?view_only=c99dd65c94b14777aa493fa6e66bd17a.** The data supporting this article has been included as part of the supplementary information (SI). See DOI: **https://doi.org/10.1039/d5sm00616c**.

## Acknowledgements

This work was financially supported by the National Science Foundation (NSF) Grant Number DMR-2142097 and the resources used were provided by Case Western Reserve University.

## Notes and references

1 S. Dhakal, Z. Chen, D. Estrin and S. Morozova, Spatially-Resolved Network Dynamics of Poly(vinyl alcohol) Gels Measured with Dynamic Small Angle Light Scattering, *Gels*, 2022, **8**, 394.
2 P. Calvert, Hydrogels for soft machines, *Adv. Mater.*, 2009, **21**, 743–756.
3 B. Erman and P. J. Flory, Critical Phenomena and Transitions in Swollen Polymer Networks and in Linear Macromolecules, *Macromolecules*, 1986, **19**, 2342–2353.
4 P. J. Flory and J. Rehner, Statistical mechanics of cross-linked polymer networks II. Swelling, *J. Chem. Phys.*, 1943, **11**, 521–526.
5 E. Geissler, F. Horkay and A. M. Hecht, Osmotic and Scattering Properties of Chemically Cross-Linked Poly(vinyl alcohol) Hydrogels, *Macromolecules*, 1991, **24**, 6006–6011.
6 F. Horkay, K. Nishi and M. Shibayama, Decisive test of the ideal behavior of tetra-PEG gels, *J. Chem. Phys.*, 2017, **146**(16), 164905.
7 L. Brannon-Peppas and N. A. Peppas, Equilibrium Swelling Behavior of pH-Sensitive Hydrogels, *Chem. Eng. Sci.*, 1991, **46**, 715–722.
8 M. Kim, S. Tang and B. D. Olsen, Physics of engineered protein hydrogels, *J. Polym. Sci., Part B: Polym. Phys.*, 2013, **51**, 587–601.
9 M. Rubinstein, R. H. Colby, A. V. Dobrynin and J. F. Joanny, Elastic modulus and equilibrium swelling of polyelectrolyte gels, *Macromolecules*, 1996, **29**, 398–406.
10 M. Rubinstein and R. H. Colby, *Polymer Physics,* Oxford Unviersity Press, 2003, ISBN 019852059X.
11 S. Hirotsu, Critical points of the volume phase transition in N-isopropylacrylamide gels, *J. Chem. Phys.*, 1988, **88**, 427–431.
12 M. Shibayama, Y. Fujikawa and S. Nomura, Dynamic Light Scattering Study of Poly(N-isopropylacrylamide-*co*-acrylic acid) Gels, *Macromolecules*, 1996, **29**, 6535–6540.
13 J. Rička and T. Tanaka, Swelling of Ionic Gels: Quantitative Performance of the Donnan Theory, *Macromolecules*, 1984, **17**, 2916–2921.
14 B. K. Roopnarine, S. C. Schmidt, K. J. Maxwell and S. Morozova, Effects of Molecular Weight and Surface Interactions on Polymer Diffusion in Confinement, *ACS Macro Lett.*, 2023, **12**, 221–226.
15 J. Gong, Y. Iwasaki, Y. Osada, K. Kurihara and Y. Hamai, Friction of Gels. 3. Friction on Solid Surfaces, *J. Phys. Chem. B*, 1999, **103**, 6001–6006.
16 Z. Cao, M. J. Stevens, J. M. Y. Carrillo and A. V. Dobrynin, Adhesion and wetting of soft nanoparticles on textured surfaces: Transition between Wenzel and Cassie-Baxter states, *Langmuir*, 2015, **31**, 1693–1703.
17 J. H. Park, Z. Schwartz, R. Olivares-Navarrete, B. D. Boyan and R. Tannenbaum, Enhancement of surface wettability via the modification of microtextured titanium implant surfaces with polyelectrolytes, *Langmuir*, 2011, **27**, 5976–5985.
18 E. R. Reale and A. C. Dunn, Poroelasticity-driven lubrication in hydrogel interfaces, *Soft Matter*, 2017, **13**, 428–435.
19 M. Krutyeva, A. Wischnewski and D. Richter, Polymer dynamics in nanoconfinement: Interfaces and interphases, *EPJ Web Conf.*, 2015, **83**, 1–5.
20 R. Michel, *et al.*, Interfacial fluid transport is a key to hydrogel bioadhesion, *Proc. Natl. Acad. Sci. U. S. A.*, 2019, **116**, 738–743.
21 C. W. Peak, J. J. Wilker and G. Schmidt, A review on tough and sticky hydrogels, *Colloid Polym. Sci.*, 2013, **291**, 2031–2047.
22 Y. Ru and M. Liu, Superwetting Gels: Wetting Principles, Applications, and Challenges, *ACS Nano*, 2025, **19**(8), 7583–7600.
23 A. Jha, P. Karnal and J. Frechette, Adhesion of fluid infused silicone elastomer to glass, *Soft Matter*, 2022, **18**, 7579–7592.
24 J. Yang, R. Bai, B. Chen and Z. Suo, Hydrogel Adhesion: A Supramolecular Synergy of Chemistry, Topology, and Mechanics, *Adv. Funct. Mater.*, 2020, **30**, 1–27.
25 J. P. Gong, Friction and lubrication of hydrogels – Its richness and complexity, *Soft Matter*, 2006, **2**, 544–552.
26 J. Gong and Y. Osada, Gel friction: A model based on surface repulsion and adsorption, *J. Chem. Phys.*, 1998, **109**, 8062–8068.
27 K. E. Jensen, *et al.*, Wetting and phase separation in soft adhesion, *Proc. Natl. Acad. Sci. U. S. A.*, 2015, **112**, 14490–14494.
28 Z. Cai, A. Skabeev, S. Morozova and J. T. Pham, Fluid separation and network deformation in wetting of soft and swollen surfaces, *Commun. Mater.*, 2021, **2**, 1–11.
29 T. Zhao, Y. Liu, Y. Wu, M. Zhao and Y. Zhao, Controllable and biocompatible 3D bioprinting technology for microorganisms: Fundamental, environmental applications and challenges, *Biotechnol. Adv.*, 2023, **69**, 108243.

30 K. T. Dicker, *et al.*, Hyaluronan: A simple polysaccharide with diverse biological functions, *Acta Biomater.*, 2014, **10**, 1558–1570.
31 F. Horkay, P. J. Basser, A. M. Hecht and E. Geissler, Gel-like behavior in aggrecan assemblies, *J. Chem. Phys.*, 2008, **128**(13), 135108.
32 A. V. Dobrynin and M. Rubinstein, Theory of polyelectrolytes in solutions and at surfaces, *Prog. Polym. Sci.*, 2005, **30**, 1049–1118.
33 W. Oppermann, *Swelling Behavior and Elastic Properties of Ionic Hydrogels*, 1992, pp. 159–170, DOI: **10.1021/bk-1992-0480.ch010**.
34 S. Morozova and M. Muthukumar, Elasticity at Swelling Equilibrium of Ultrasoft Polyelectrolyte Gels: Comparisons of Theory and Experiments, *Macromolecules*, 2017, **50**, 2456–2466.
35 Y. Osada and J.-P. Gong, Soft and Wet Materials: Polymer Gels, *Adv. Mater.*, 1998, **10**, 827–837.
36 K. Bergman, C. Elvingson, J. Hilborn, G. Svensk and T. Bowden, Hyaluronic acid derivatives prepared in aqueous media by triazine-activated amidation, *Biomacromolecules*, 2007, **8**, 2190–2195.
37 J. Liang, L. Cheng, J. J. Struckhoff and N. Ravi, Investigating triazine-based modification of hyaluronan using statistical designs, *Carbohydr. Polym.*, 2015, **132**, 472–480.
38 T. Borke, F. M. Winnik, H. Tenhu and S. Hietala, Optimized triazine-mediated amidation for efficient and controlled functionalization of hyaluronic acid, *Carbohydr. Polym.*, 2015, **116**, 42–50.
39 K. Thompson and S. Michielsen, Novel synthesis of N-substituted polyacrylamides: Derivatization of poly(acrylic acid) with amines using a triazine-based condensing reagent, *J. Polym. Sci., Part A: Polym. Chem.*, 2006, **44**, 126–136.
40 S. H. Behrens and D. G. Grier, The charge of glass and silica surfaces, *J. Chem. Phys.*, 2001, **115**, 6716–6721.
41 Z. Fan, *et al.*, UV/ozone-assisted rapid formation of high-quality tribological self-assembled monolayer, *Coatings*, 2019, **9**, 1–10.
42 T. Tanaka, L. O. Hocker and G. B. Benedek, Spectrum of light scattered from a viscoelastic gel, *J. Chem. Phys.*, 1973, **59**, 5160–5183.
43 M. Shibayama, Spatial inhomogeneity and dynamic fluctuations of polymer gels, *Macromol. Chem. Phys.*, 1998, **199**, 1–30.
44 T. Hiroi, M. Ohl, T. Sakai and M. Shibayama, Multiscale dynamics of inhomogeneity-free polymer gels, *Macromolecules*, 2014, **47**, 763–770.
45 M. S. Safari, M. A. Vorontsova, R. Poling-Skutvik, P. G. Vekilov and J. C. Conrad, Differential dynamic microscopy of weakly scattering and polydisperse protein-rich clusters, *Phys. Rev. E: Stat., Nonlinear, Soft Matter Phys.*, 2015, **92**(4), 042712.
46 M. S. Safari, R. Poling-Skutvik, P. G. Vekilov and J. C. Conrad, Differential dynamic microscopy of bidisperse colloidal suspensions, *npj Microgravity*, 2017, **3**, 21.
47 J. D. C. Jacob, K. He, S. T. Retterer, R. Krishnamoorti and J. C. Conrad, Diffusive dynamics of nanoparticles in ultra-confined media, *Soft Matter*, 2015, **11**, 7515–7524.
48 K. He, M. Spannuth, J. C. Conrad and R. Krishnamoorti, Diffusive dynamics of nanoparticles in aqueous dispersions, *Soft Matter*, 2012, **8**, 11933–11938.
49 E. Hitimana, B. K. Roopnarine and S. Morozova, Diffusive dynamics of charged nanoparticles in convex lens-induced confinement, *Soft Matter*, 2022, **18**, 832–840.
50 G. Nisato, F. Schosseler and S. J. Candau, Swelling Equilibrium Properties of Partially Charged Gels: The Effect of Salt on the Shear Modulus, *Polym. Gels Networks*, 1996, **4**, 481–498.
51 M. Muthukumar, *Physics of Charged Macromolecules: Synthetic and Biological Systems*, 2023.
52 A. Daoui and P. Snabre, Poroviscoelasticity and compression-softening of agarose hydrogels, *Rheol. Acta*, 2021, **60**, 327–351.
53 K. G. Wilcox, S. K. Kozawa and S. Morozova, Fundamentals and mechanics of polyelectrolyte gels: Thermodynamics, swelling, scattering, and elasticity, *Chem. Phys. Rev*, 2021, **2**, 041309.
54 W. Zhao, J. Zhou, H. Hu, C. Xu and Q. Xu, The role of crosslinking density in surface stress and surface energy of soft solids, *Soft Matter*, 2022, **18**, 507–513.

 